

# Osmotic Swelling to Exfoliation. Exceptionally High Degrees of Hydration of a Layered Titanate

Takayoshi Sasaki\* and Mamoru Watanabe

Contribution from the National Institute for Research in Inorganic Materials,  
1-1 Namiki, Tsukuba, Ibaraki 305-0044, Japan

Received December 16, 1997

**Abstract:** This paper describes the swelling/exfoliation process in which a layered protonic titanate,  $H_xTi_{2-x/4}\square_{x/4}O_4 \cdot H_2O$  ( $x \sim 0.7$ ;  $\square$ , vacancy), undergoes high degrees of hydration in aqueous media containing tetrabutylammonium (abbreviated as TBA hereafter) ions. A high content of electrolyte (25-fold excess of TBA ions to the exchangeable protons in the titanate) induced the formation of an osmotically swollen hydrate yielding a well-defined basal diffraction series. Intersheet separation of 4.2 nm at this stage expanded further to exceed 10 nm with reducing the dose of TBA ions. Along this swelling, exfoliation into single sheets became prevalent while the swollen component declined. This was followed by X-ray diffraction data for wet colloids centrifuged from suspensions that revealed a broad diffraction envelope besides the sharp basal reflections. Profile simulations demonstrated that the hump is attributable to scattering from a pile of exfoliated nanosheets and that its appearance is diagnostic for delamination. The TBA content approximately half-equivalent to the exchangeable protons was found to be a threshold for delamination below which the usual intercalation reaction occurred. This threshold corresponds to stoichiometry where the nanosheet surface is effectively covered with TBA ions. The UV–visible spectra for colloidal suspensions revealed an absorption peak at 265 nm, the intensity of which increased until the TBA content decreased to 5-fold excess of an equivalent of the exchange capacity. The background varied in a contrary manner. These changes can be interpreted as a reflection of a process whereby the parent crystals were cleaved into thinner crystallites and eventually elementary host sheets.

## Introduction

Recently it has been reported that a variety of layered compounds were delaminated into their elementary host layers by controlling layer-to-layer interactions via soft-chemical procedures.<sup>1–8</sup> The resultant colloidal nanosheets are taken as a new class of inorganic macromolecules having a two-dimensional crystalline lattice whose thickness ranges from subnanometer to nanometer scale. Their molecular nature is

expected to evolve distinctive chemical and physical properties. In view of material synthesis, the exfoliated nanosheets are useful as building blocks for new materials which cannot be realized via other processes. Nanocomposites of inorganic layered hosts with bulky guests have been prepared by reassembling the nanosheets in their presence. Organic polymers and polyoxocations have been incorporated into the gallery via this strategy.<sup>9–11</sup> Moreover, novel functionalized systems have been constructed by layer-by-layer manipulation based on self-assembly techniques.<sup>12,13</sup> Most recently, exfoliation has been applied to shape-control particulates. Thin  $TiO_2$  flakes tens-nanometers thick have been fabricated by freeze-drying colloidal suspensions of an exfoliated titanate and subsequent heating.<sup>14</sup>

Because the exfoliated nanosheet crystallites are attractive, it is important to understand how a layered structure is separated

- (1) Jacobson, A. J. *Mater. Sci. Forum* **1994**, 152–153, 1–12.  
 (2) (a) Murphy, D. W.; Hull, G. W., Jr. *J. Chem. Phys.* **1975**, 62, 973–978. (b) Lerf, A.; Schöllhorn, R. *Inorg. Chem.* **1977**, 16, 2950–2956.  
 (3) (a) Nadeau, P. H.; Wilson, M. J.; McHardy, W. J.; Tait, J. M. *Science* **1984**, 225, 923–925. (b) Nadeau, P. H.; Tait, J. M.; McHardy, W. J.; Wilson, M. J. *Clay Minerals* **1984**, 19, 67–76. (c) Nadeau, P. H.; Wilson, M. J.; McHardy, W. J.; Tait, J. M. *Clay Minerals* **1984**, 19, 757–769.  
 (4) (a) Liu, C.; Singh, O.; Joensen, P.; Curzon, A. E.; Frindt, R. F. *Thin Solid Films* **1984**, 113, 165–172. (b) Joensen, P.; Frindt, R. F.; Morrison, S. R. *Mater. Res. Bull.* **1986**, 21, 457–461. (c) Joensen, P.; Crozier, E. D.; Alberding, N.; Frindt, R. F. *J. Phys. C: Solid State Phys.* **1987**, 20, 4043–4053. (d) Yang, D.; Jiménez Sandoval, S.; Divigalpitaya, W. M. R.; Irwin, J. C.; Frindt, R. F. *Phys. Rev. B* **1991**, 43, 12053–12056. (e) Yang, D.; Frindt, R. F. *J. Phys. Chem. Solids* **1996**, 57, 1113–1116.  
 (5) Bonneau, P.; Mansot, J. L.; Rouxel, J. *Mater. Res. Bull.* **1993**, 28, 757–766.  
 (6) (a) Alberti, G.; Casciola, M.; Costantino, U. *J. Colloid Interface Sci.* **1985**, 107, 256–263. (b) Alberti, G.; Dionigi, C.; Giontella, E.; Murcia-Mascaros, S. *J. Colloid Interface Sci.* **1997**, 188, 27–31. (c) Alberti, G.; Giontella, E.; Murcia-Mascaros, S. *Inorg. Chem.* **1997**, 36, 2844–2849.  
 (7) (a) Treacy, M. M.; Rice, S. B.; Jacobson, A. J.; Lewandowski, J. T. *Chem. Mater.* **1990**, 2, 279–286. (b) Domen, K.; Ebina, Y.; Ikeda, S.; Tanaka, A.; Kondo, J. N.; Maruya, K. *Catal. Today* **1996**, 28, 264–274.  
 (8) (a) Sasaki, T.; Watanabe, M.; Hashizume, H.; Yamada, H.; Nakazawa, H. *J. Chem. Soc., Chem. Commun.* **1996**, 229–230. (b) Sasaki, T.; Watanabe, M.; Hashizume, H.; Yamada, H.; Nakazawa, H. *J. Am. Chem. Soc.* **1996**, 118, 8329–8335.

- (9) (a) Divigalpitaya, W. M. R.; Frindt, R. F.; Morrison, S. R. *Science* **1989**, 246, 369–371. (b) Kanatzidis, M. G.; Bissessur, R.; DeGroot, D. C.; Schindler, J. L.; Kannewurf, C. R. *Chem. Mater.* **1993**, 5, 595–596. (c) Nazar, L. F.; Jacobson, A. J. *J. Mater. Chem.* **1994**, 4, 1419–1425.  
 (10) (a) Divigalpitaya, W. M. R.; Frindt, R. F.; Morrison, S. R. *J. Mater. Res.* **1991**, 6, 1103–1107. (b) Wu, J.; Lerner, M. M. *Chem. Mater.* **1993**, 5, 835–838. (c) Lemmon, J. P.; Lerner, M. M. *Chem. Mater.* **1994**, 6, 207–210. (d) Lemmon, J. P.; Wu, J.; Oriakhi, C. O.; Lerner, M. M. *Electrochim. Acta* **1995**, 40, 2245–2249. (e) Oriakhi, C. O.; Nafshun, R. L.; Lerner, M. M. *Mater. Res. Bull.* **1996**, 31, 1513–1520. (f) Wang, L.; Schindler, J.; Kannewurf, C. R.; Kanatzidis, M. G. *J. Mater. Chem.* **1997**, 7, 1277–1283.  
 (11) Nazar, L. F.; Liblong, S. W.; Yin, X. T. *J. Am. Chem. Soc.* **1991**, 113, 5889–5890.  
 (12) Kleinfeld, E. R.; Ferguson, G. S. *Science* **1994**, 265, 370–373.  
 (13) Keller, S. W.; Kim, H.-N.; Mallouk, T. E. *J. Am. Chem. Soc.* **1994**, 116, 8817–8818.  
 (14) Sasaki, T.; Nakano, S.; Yamauchi, S.; Watanabe, M. *Chem. Mater.* **1997**, 9, 602–608.

into single sheets. Such information is of fundamental interest to grasp the nature of layered systems and can help in designing experimental procedures to exfoliate layered materials which have not been delaminated.

Most studies on exfoliation have focussed on the phenomenon itself, delamination techniques, and material syntheses from delaminated crystallites. There have been only a few reports treating the chemistry of the swelling process to exfoliation. Alberti et al. found that  $\alpha$ -zirconium phosphate became colloidal in the course of titration with *n*-propylamine. They showed that the length of alkyl chain and an appropriate range of titration (30–50% consumption of the cation exchange capacity) were important for the phenomenon. The colloidal suspension was neither obtained with *n*-alkylamines having a longer chain nor outside the above compositional range with *n*-propylamine. These data imply that there are critical conditions for delamination which must be fulfilled. However, this paper does not describe how swelling proceeds to exfoliation.

Swelling via hydration has been examined extensively with respect to clay minerals. They undergo hydration when brought into contact with atmospheric humidity or an aqueous phase. The interlayer distance expands in a stepwise fashion, corresponding to incorporating multiple integral layers of water molecules into the gallery. Mono-, bi-, and trilayer hydrates have been reported for a number of layered materials as well as clay minerals.<sup>15–18</sup>

In addition to normal crystalline swelling, there is another type of swelling, much higher degrees of intersheet expansion via osmotic hydration.<sup>15a,19,20</sup> Upon contact with an aqueous solution of certain electrolytes, a large volume of water is introduced into the gallery, resulting in an interlayer separation of usually >2 nm and exceeding 20 nm in extreme cases. Delamination into single sheets may be considered as the ultimate stage of the osmotic swelling process, in other words, infinite swelling. However, it remains unclear how osmotic swelling and exfoliation reactions interrelate.

Difficulties in characterizing the swelling phenomenon in this range are associated with the following: (i) Observations of osmotic swelling have been limited to clay minerals such as smectites and vermiculites.<sup>15a,19,20</sup> To our knowledge, there has been no report on this phenomenon for other layered hosts even those for which exfoliation has been demonstrated. In general, clay minerals are poorly crystalline, showing broad diffraction patterns. This tendency is particularly enhanced when highly

swollen. (ii) Osmotically swollen phases occur as colloidal suspensions. It is essential to examine a sample as is since osmotic swelling collapses on drying. These circumstances impede elaborate analysis of swollen hydrates.

Recently we reported that a layered protonic titanate,  $H_xTi_{2-x/4}\square_{x/4}O_4 \cdot H_2O$ , with lepidocrocite-type structure can be exfoliated into single sheets on the action of an aqueous solution containing bulky quarternary alkylammonium ions.<sup>8</sup> A dynamic reassembling process of titanate nanosheets was followed by an in situ X-ray diffraction study. Owing to high crystallinity, the colloidal titanate produced well-defined diffraction patterns, which made the analysis facile. This can also be expected for osmotic swelling in this system. The present study is undertaken to gain an insight into the osmotic swelling and exfoliation process by characterizing the high hydration states of the titanate.

## Results and Analysis

**Electrolyte Concentration Dependence on Swelling.** We examined the swelling behavior of  $H_xTi_{2-x/4}\square_{x/4}O_4 \cdot H_2O$  ( $x = 0.7$ ) equilibrated with aqueous solutions of TBA hydroxide. The molar ratio of TBA ions over exchangeable protons in  $H_xTi_{2-x/4}\square_{x/4}O_4 \cdot H_2O$ , referred to as  $TBA^+/H^+$ , ranged from 0.1 to 25. Samples with  $TBA^+/H^+ \geq 0.5$  produced colloidal suspensions on shaking which were stable without noticeable sedimentation. The only exception was the sample with the lowest TBA content ( $TBA^+/H^+ = 0.1$ ), where separation into solid and supernatant solution took place on standing. Intermediate behavior was observed in the sample with  $TBA^+/H^+ = 0.3$ . The appearance of colloidal suspensions depended on TBA content. Color tended to change from opalescent to translucent as the value of  $TBA^+/H^+$  decreased from 25 to ~5. Translucency remained almost unchanged in the  $TBA^+/H^+$  range of 1–5 and was lost again in the samples with  $TBA^+/H^+ < 1$ .

Figure 1 shows typical X-ray diffraction patterns for the colloidal suspensions themselves. The data for  $H_xTi_{2-x/4}\square_{x/4}O_4 \cdot H_2O$  is also given for purposes of comparison. All samples displayed a broad diffraction halo in a  $2\theta$  range of 20–50° characteristic of aqueous solutions. Besides this diffraction feature, sharp basal diffraction series were observed in a low angular range when a high dose of TBA ions was applied. The suspension with  $TBA^+/H^+ = 25$  revealed a gallery height of 4.2 nm, which largely expanded from the original value of 0.94 nm for  $H_xTi_{2-x/4}\square_{x/4}O_4 \cdot H_2O$ . This expansion cannot be explained merely by the introduction of TBA ions into interlayer space. Gallery height may be accounted for by uptake of a large amount of water, nominally > 10 layers of  $H_2O$  molecules. Swelling collapsed on drying, as will be described later. Thus the obtained pattern is ascribable to osmotic swelling.

As the TBA content was reduced, the intensity of basal reflections diminished and were not detectable in the suspensions with  $TBA^+/H^+ < 10$ . On the other hand, sharp diffraction lines were discerned, as designated by arrows, for the sample having the lowest TBA content. One had a spacing of 0.94 nm, indicating the presence of protonic titanate. The other line of 1.63 nm may have resulted from titanate intercalated with TBA ions. Its identification will be detailed later.

X-ray diffraction patterns for colloidal aggregates centrifuged from the suspensions are depicted in Figures 2 and 3, which were not disturbed by a strong signal from the aqueous phase and lack of sensitivity owing to a low titanate content. Data for the sample with  $TBA^+/H^+ = 25$  comprised sharp basal reflections. Its intersheet spacing of 4.2 nm was exactly equal

(15) (a) MacEwan, D. M. C.; Wilson, M. J. *Crystal Structures of Clay Minerals and Their X-Ray Identification*; Brindley, G. W., Brown, G., Eds.; Mineralogical Society: London, 1980. (b) Glaeser, R.; Méring, J. C. R. *Held. Séanc. Acad. Sci., Paris* **1968**, *267*, 436–466. (c) Moore, C. M.; Hower, J. *Clays Clay Miner.* **1986**, *34*, 379–384. (d) Watanabe, T.; Sato, T. *Clay Sci.* **1988**, *7*, 129–138. (e) Yamada, H.; Nakazawa, H.; Hashizume, H.; Shimomura, S.; Watanabe, T. *Clays Clay Miner.* **1994**, *42*, 77–80.

(16) Schöllhorn, R. *Intercalation Chemistry*; Whittingham, M. S., Jacobson, A. J., Eds.; Academic Press: New York, 1982.

(17) (a) Sasaki, T.; Watanabe, M.; Komatsu, Y.; Fujiki, Y. *Inorg. Chem.* **1985**, *24*, 2265–2271. (b) Sasaki, T.; Watanabe, M.; Komatsu, Y.; Fujiki, Y. *Bull. Chem. Soc. Jpn.* **1985**, *58*, 3500–3505. (c) Sasaki, T.; Komatsu, Y.; Fujiki, Y. *Mater. Res. Bull.* **1987**, *22*, 1321–1328. (d) Sasaki, T.; Komatsu, Y.; Fujiki, Y. *Inorg. Chem.* **1989**, *28*, 2776–2779. (e) Sasaki, T.; Komatsu, Y.; Fujiki, Y. *Chem. Mater.* **1992**, *4*, 894–899.

(18) (a) Sasaki, T.; Komatsu, Y.; Fujiki, Y. *J. Chem. Soc., Chem. Commun.* **1991**, 817–818. (b) Sasaki, T.; Watanabe, M.; Michiue, Y.; Komatsu, Y.; Izumi, F.; Takenouchi, S. *Chem. Mater.* **1995**, *7*, 1001–1007.

(19) (a) Norrish, K. *Discuss. Faraday Soc.* **1954**, *18*, 120–134. (b) Foster, W. R.; Savins, J. E.; Waite, J. M. *Clays Clay Miner.* **1955**, *3*, 296–316. (c) Fukushima, Y. *Clays Clay Miner.* **1984**, *32*, 320–326.

(20) (a) Walker, G. F. *Nature* **1960**, *187*, 312–313. (b) Viani, B. E.; Roth, C. B.; Low, P. F. *Clays Clay Miner.* **1985**, *33*, 244–250. (c) Braganza, L. F.; Crawford, R. J.; Smalley, M. V.; Thomas, R. K. *Clays Clay Miner.* **1990**, *38*, 90–96.

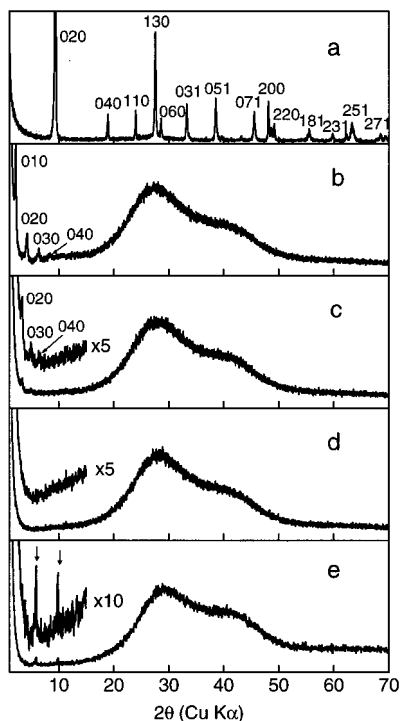


**Figure 1.** X-ray diffraction patterns: (a) for the protonic titanate of  $H_xTi_{2-x/4}□_{x/4}O_4 \cdot H_2O$  and (b)–(e) for colloidal suspensions with various TBA contents. The molar ratio of TBA ions over exchangeable protons in the titanate,  $TBA^+/H^+$ , is 25 for (b), 15 for (c), 5 for (d) and 0.1 for (e). The indices given in (a) are based on the orthorhombic layered structure with unit-cell parameters of  $a = 0.3783(2)$  nm,  $b = 1.8735(8)$  nm, and  $c = 0.2978(2)$  nm.

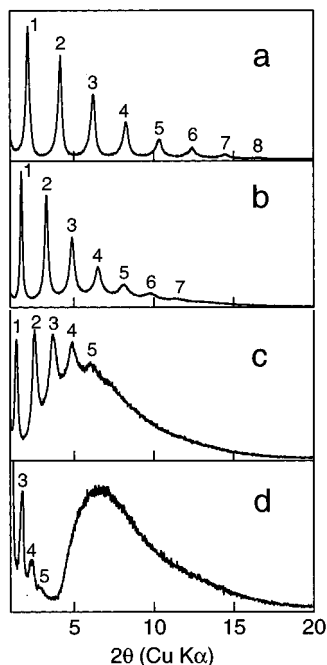


**Figure 2.** X-ray diffraction patterns for a colloidal aggregate centrifuged from suspensions with various TBA content. The molar ratio of  $TBA^+/H^+$  is 25 for (b), 15 for (c), 10 for (d), and 2 for (e). The numeral at each peak designates the order of basal reflections.

to the value obtained from the data for the aqueous suspension itself (Figure 1b), showing that equilibrium swelling was preserved after centrifugation.

Sharp diffraction lines up to the eighth order indicated a highly ordered hydrate structure, in striking contrast to the case

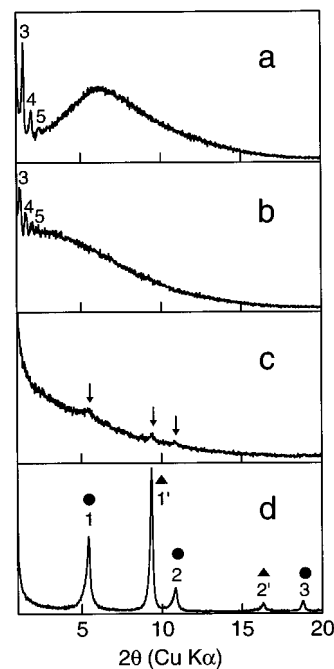


**Figure 3.** X-ray diffraction patterns for a colloidal aggregate centrifuged from suspensions with  $TBA^+/H^+ = 1$  for (a), 0.5 for (b), 0.3 for (c), and 0.1 for (d). Two sets of diffraction series in (d), designated by circles and triangles, have a basal spacing of 1.63 and 0.94 nm, respectively.

of swollen clay minerals. Smectites usually yield diffuse diffraction patterns with one or two broad maxima when osmotically swollen. Their diffraction feature was not ascribed to single intersheet spacing but to statistical distribution of it.<sup>15a,19a</sup>

A decrease in TBA concentration brought about a steady increase in intersheet separation which finally exceeded 10 nm. Another noticeable feature was evolution of an amorphouslike halo in a  $2\theta$  range of  $3\text{--}20^\circ$ , which is most prominent in Figure 2d. This broad diffraction envelope is due to scattering from an aggregate of exfoliated titanate sheets, a detailed analysis of which will be presented in the next section.

Osmotic hydration appeared to progress further for samples centrifuged from the suspensions with  $TBA^+/H^+ \leq 1$  (see Figure 3). However, diffraction peaks associated with the swollen component gradually diminished in this process and disappeared at  $TBA^+/H^+ = 0.3$ , where two sets of basal reflection series emerged faintly in addition to the broad pattern. The sample having the lowest TBA content comprised these two crystalline phases with an interlayer distance of 1.63 and 0.94 nm. These values are identical to those observed in the aqueous slurry (Figure 1e). Disappearance of the broad pattern along with the increase of crystalline phases suggests that the system no longer was colloidal.

The swelling state in aqueous media can be pursued by examining dried products. Irrespective of various degrees of swelling, the samples with  $TBA^+/H^+ \geq 1$  produced the same well-ordered lamellar structure with a repeat distance of 1.75 nm as shown in Figure 4. This phase has been identified as a TBA complex of the titanate.<sup>14,21</sup> The sample with  $TBA^+/H^+ = 0.5$  also resulted in an identical 1.75 nm phase except for its slight degradation of crystallinity. On the other hand, there were two immiscible phases, expanded (1.63 nm) and nonexpanded (0.94 nm), for the dried product of  $TBA^+/H^+ = 0.1$ . The X-ray

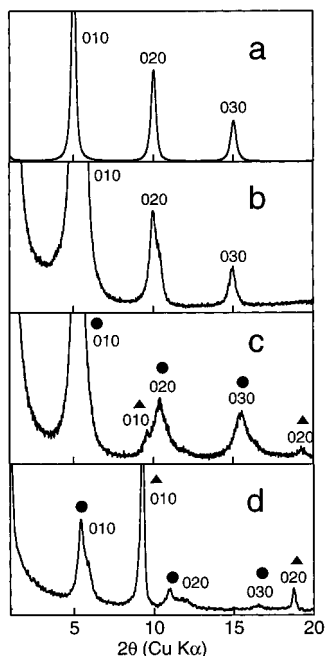


**Figure 4.** X-ray diffraction patterns for air-dried products from the colloidal suspension with  $\text{TBA}^+/\text{H}^+ = 1$  for (a), 0.5 for (b), 0.3 for (c), and 0.1 for (d). Intensity ranges in (a) and (b) are 10 and 2 times those in (c) and (d). The data in (c) and (d) indicate the presence of two immiscible phases as designated by circles and triangles.

diffraction data changed only negligibly on drying (compare Figure 4d with Figures 1e and 3d). The expanded and nonexpanded phases may be described as a TBA intercalated material and unreacted protonic titanate, respectively. The latter phase persisted in the sample with  $\text{TBA}^+/\text{H}^+ = 0.3$ , coexisting with a dominant component of 1.68 nm.

These marked changes which occurred at  $\text{TBA}^+/\text{H}^+ = 0.3$ –0.5 strongly suggest that the samples with  $\text{TBA}^+/\text{H}^+ \geq 0.5$  are colloidal while those with  $\text{TBA}^+/\text{H}^+ \leq 0.3$  are a mixture of solid and solution. Protonic titanate was present only in the latter samples. Noticeable differences in crystallinity and gallery height of the expanded phase can also be understood in terms of the formation limit of colloidal suspension. Formation of the 1.75 nm phase involves collapse of osmotically swollen hydrates owing to loss of water from the intersheet domain and also restacking of the exfoliated sheets, if any, by accommodating TBA ions. The reaction through this route is likely to take place homogeneously among the intersheet spaces throughout a crystallite and produces the well-ordered lamellar structure experimentally observed. Conversely, basal reflections of the corresponding phase for  $\text{TBA}^+/\text{H}^+ \leq 0.3$  were broad, which was enhanced to have a shoulder for  $\text{TBA}^+/\text{H}^+ = 0.1$ . Heterogeneity associated with random and/or segregative interstratification may be responsible for this feature. A mixed-layered system of two spacings, 1.75 and 0.94 nm, can reasonably elucidate an apparent shift of gallery height from 1.63 to 1.68 nm, then to 1.75 nm with the increase of  $\text{TBA}^+/\text{H}^+$ ;  $0.1 \rightarrow 0.3 \rightarrow \geq 0.5$ . This inhomogeneity, associated with a smaller amount of guests, tends to appear in the solid/solution interaction process where guest molecules diffuse into crystalline lattices from solutions.

**Analysis of the Diffraction Envelope.** To understand the swelling/exfoliation process, it is essential to clarify what arises the distinctive diffraction halo. The TBA aqueous solution itself is not responsible for this diffraction because it does not produce

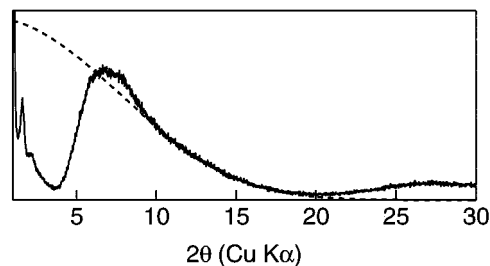


**Figure 5.** Square of calculated structure factor for the nanosheets and a typical experimental profile of the diffraction envelope. The former is expressed by a broken line.

a halo in this angular range, as shown in Figure 1. Accordingly, the observed pattern should be related to scattering from the titanate.

Figure 5 compares typical experimental data with the square of structure factor,  $F^2(\theta)$ , for the nanosheet of composition,  $\text{Ti}_{2-x/4}\text{V}_{x/4}\text{O}_4^{x-}$ . The calculated pattern corresponds to what is expected for the nanosheets that individually scatter without phase interaction. The observed data is superimposable on this calculated trace particularly in a higher angle region. This strongly suggests that the broad envelope of scattering arises from nanosheets assembled in a disordered manner. A deviation in a lower angular range, that is, a drop nearly to the baseline, points to a certain interference between the nanosheets. Note that scattering from the nanosheets causes mutual interference when in parallel configuration.

To obtain a semiquantitative picture of the assembly state of nanosheets, X-ray diffraction profiles were simulated for stacked nanosheets, the separation of which was assumed to fluctuate around the most probable value,  $d$ , according to Gaussian distribution with the standard deviation of  $\alpha$ . Typical simulated results are summarized in Figures 6 and 7. For a small value of  $\alpha$ , the pattern is of normal Bragg reflections, the higher orders of which are broadened by a strain broadening effect. As  $\alpha$  increases, the higher-angular-range profile approaches the trace of  $F^2(\theta)$ . The profile is less sensitive to the number of titanate sheets especially for large values of  $\alpha$  (see Figure 7). The parameters of  $d = 1.2$  nm and  $\alpha = 0.5$ –1.0 nm appeared to satisfactorily reproduce the experimental data. Figure 8 visualizes a probability of nanosheet occurrence at a certain distance from a specified one, which was calculated by convolution of Gaussian distribution function with these parameters. It is clear that for a most likely value of  $\alpha$ , 0.75 nm, sheet distribution is almost flat save for the vicinity of origin. This indicates that nanosheets arrange themselves in a nearly amorphous manner except for nearest-neighbor correlation. These circumstances are comparable to liquids and high-pressure gas phases. Strictly speaking, symmetrical distribution, such as Gaussian function, is not realistic since proximity of two nanosheets leading to overlap should not be allowed. Nevertheless, we consider that the calculations here are helpful to understand the state of aggregation.

Nanosheets are piled intimately as a result of centrifugation. Removal of most of the water from colloidal suspensions may result in parallel piling as the most stable configuration for the anisotropic shape of nanosheets. It should be pointed out that the broad diffraction hump in terms of the lower-angle profile and the peak position was variable, being dependent on conditions for centrifugation (speed and duration) as well as TBA concentration in the suspensions. Such examples can be

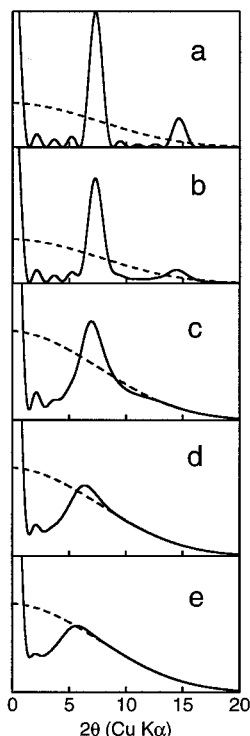


**Figure 6.** Simulated X-ray diffraction profiles for the five parallel nanosheets having various degrees of disorder in intersheet separation. Average intersheet spacing is 1.2 nm. The mean displacement of  $\alpha$  for (a)–(e) is 0, 0.2, 0.5, 0.75, and 1.0 nm, respectively. The dashed trace denotes  $F^2(\theta)$  for the nanosheet. Intensity scale in (a) and (b) is five times that in (c)–(e).

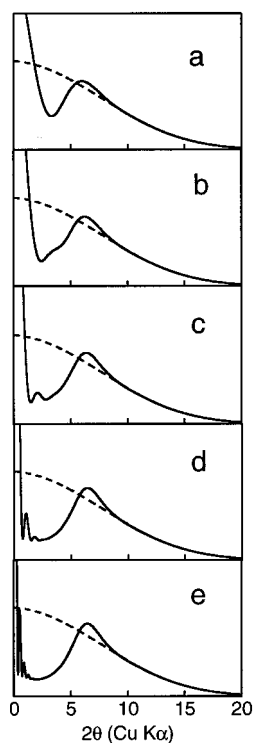


**Figure 7.** Simulated X-ray diffraction profiles as a function of the number of stacked nanosheets. Stacking numbers for (a)–(e) are 2, 3, 5, 10, and 20, respectively. Average intersheet spacing and standard deviation are 1.2 and 0.75 nm, respectively.

found in Figures 2 and 3. This behavior is reasonable as the state of aggregation should be sensitive to the factors of how the nanosheets were collected.

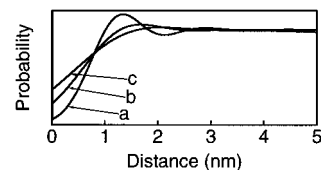


**Figure 8.** Distribution of nanosheets from one sheet. Average intersheet separation is 1.2 nm. Its mean displacement for (a)–(c) is 0.5, 0.75, and 1.0 nm, respectively.

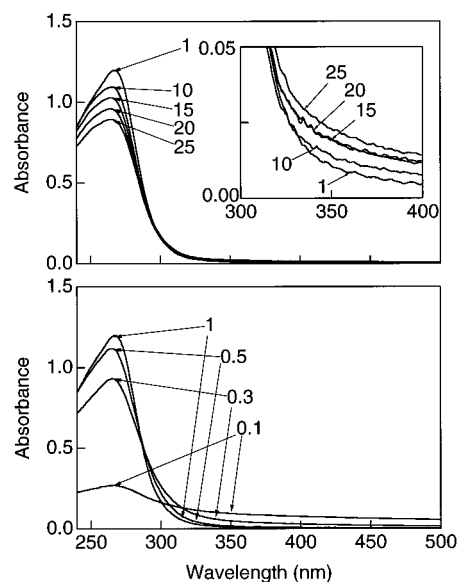


**Figure 9.** UV–visible spectra for colloidal suspensions at various TBA concentrations. Numerals represent the molar ratio of  $\text{TBA}^+/\text{H}^+$ . The titanate content was  $0.012 \text{ g dm}^{-3}$  for all samples.

To sum up, the diffraction envelope can be interpreted as scattering from the nanosheets stacked irregularly as a result of centrifugation. These nanosheets most likely were dispersed as individual molecular species in the colloidal suspensions. Consequently, the broad diffraction feature can be taken as “fingerprint” evidence of exfoliation into single sheets.

**UV–Visible Absorption Spectra.** Figure 9 illustrates the optical absorption spectra for the colloidal suspensions which revealed characteristic features for semiconductors. The sharp threshold and its marked blue shift compared with bulk  $\text{TiO}_2$  and the parent crystals of  $\text{H}_x\text{Ti}_{2-x/4}\square_{x/4}\text{O}_4 \cdot \text{H}_2\text{O}$  may be due to the molecular nature of the delaminated nanosheets and their size quantization.<sup>22</sup> Points to be focussed on here are changes in absorption intensities in the course of swelling. The peak-top absorbance at 265 nm increased when lowering the value of  $\text{TBA}^+/\text{H}^+$  from 25 to 10. By contrast, the order was reversed for the baseline data around 350 nm. The data in the  $\text{TBA}^+/\text{H}^+$  range of 1–5 agreed with each other within experimental error. The reverse situation to the suspensions with  $\text{TBA}^+/\text{H}^+ \geq 10$  was true for  $\text{TBA}^+/\text{H}^+ \leq 1$ . As the TBA content fell, the peak-top absorbance diminished while the background became higher. These changes paralleled the appearance of the suspensions as visually observed.

It has been demonstrated that oscillator strength for quantum-sized semiconductors grows as crystallite size decreases.<sup>23</sup> Therefore, peak-top absorbance should closely relate to the degree of exfoliation. On the other hand, apparent absorption

(22) Sasaki, T.; Watanabe, M. *J. Phys. Chem. B* **1997**, *101*, 10159–10161.

(23) Vossmeier, T.; Katsikas, L.; Giersig, M.; Popovic, I. G.; Diesner, K.; Chemseddine, A.; Eychmüller, A.; Weller, H. *J. Phys. Chem.* **1994**, *98*, 7665–7673.

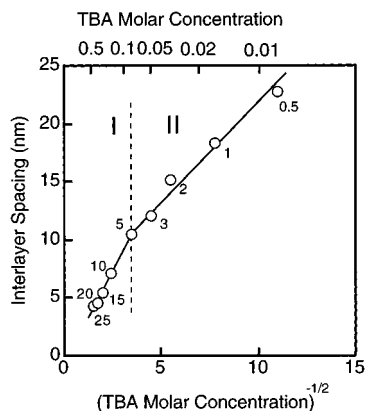


**Figure 10.** Intersheet spacing as a function of the reciprocal of the square root of TBA concentration. Numerals represent the ratio of  $\text{TBA}^+/\text{H}^+$ .

in the baseline region may be accounted for primarily by the contribution of light scattering by large particles. The high background for the samples with high TBA contents and those with  $\text{TBA}^+/\text{H}^+ \leq 0.3$  may be associated with the presence of osmotically swollen crystallites and large particles which are not delaminated, respectively. Accordingly, the changes in the optical absorption properties may be employed as an experimental measure displaying the degree of swelling.

### Discussion

Although the hydration phenomena of crystalline swelling have been studied in a number of layered host materials,<sup>15–18</sup> osmotic swelling has not been explored extensively, the present data being the first except for clay minerals. The X-ray diffraction data, which are well-defined compared with those for clay minerals, definitely indicates that TBA concentration dominates the swelling/exfoliation process. Osmotic swelling was predominant at a higher TBA dose, and exfoliation into single sheets was promoted at a lower concentration. The following discussion will focus on the relationship between osmotic swelling and exfoliation.

Basal spacing for the osmotically swollen phase detected in centrifuged colloidal aggregate is plotted against the reciprocal of the square root of TBA molar concentration (Figure 10), which gives two linear relationships. Studies of clay minerals established that the degree of osmotic swelling is inversely proportional to the square root of electrolyte concentrations.<sup>15,16</sup> For example, Norrish demonstrated this linear relationship for montmorillonite in aqueous  $\text{NaCl}$  and  $\text{Na}_2\text{SO}_4$  solutions.<sup>15b</sup> This behavior has been shown to be consistent with the theory on colloids (DLVO) that colloidal particles in aqueous suspensions are blanketed with electrical double layers whose thickness changes in a manner described above.

The osmotic swelling for the present system seems to be divided into two regions since the linear relationships in Figure 10 show a distinct change in slope at  $\text{TBA}^+/\text{H}^+ \sim 5$ . The data in the high TBA-content region, Domain I, represent genuine osmotic swelling or equilibrium swelling. It should be remembered that the same intersheet spacing was obtained for the aqueous suspensions themselves and for the colloids after centrifugation. As osmotic expansion progressed with the decrease of TBA content, exfoliation into single sheets became significant. Note that the diffraction envelope was already detectable at  $\text{TBA}^+/\text{H}^+ = 15$  (Figure 2).<sup>24</sup>

(24) The scale in Figure 2b is five times that in Figure 2c.

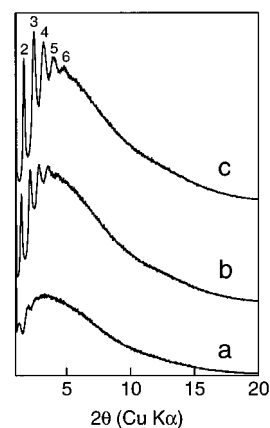


**Figure 11.** Time evolution of the osmotic swelling after centrifugation from the aqueous suspension with  $\text{TBA}^+/\text{H}^+ = 2$ : (a) 1 min, (b) 70 min, and (c) 140 min.

We presume that in Domain II ( $\text{TBA}^+/\text{H}^+ < 5$ ) the layered structure was completely exfoliated, and the resulting nanosheets were dispersed in the aqueous medium. This is based on the following facts: (i) Corresponding sharp reflections were absent in the aqueous suspensions (Figure 1). (ii) A predominant feature in X-ray diffraction data for the colloidal aggregate centrifuged from the suspensions was the broad envelope. (iii) UV-visible spectra, a monitor of the degree of exfoliation, did not change appreciably in the  $\text{TBA}^+/\text{H}^+$  range of 0.5–5.

Then what generated the sharp basal reflections in Domain II? It existed only in a trace amount and may not represent equilibrium swelling. Rather, the basal diffraction series in this region may be ascribed to osmotic swelling reorganized from the dispersed nanosheets. It took about a minute to load the centrifuged colloid onto the diffractometer with a humidity-controllable chamber. This procedure inevitably exposed the sample to ambient atmosphere, which may have partially dried its surface and produced osmotic swelling on local equilibration with a new chemical environment. This is clearly seen by time evolution of X-ray diffraction profiles after centrifugation (Figure 11). Only a negligible amount of the osmotically swollen phase was observed in the colloidal aggregate immediately after centrifugation. The overwhelmingly salient feature was the broad hump, suggesting that a majority of titanate sheets were delaminated. Given time, the sharp basal reflections developed significantly.<sup>25</sup> These data strongly support the hypothesis that a swollen hydrate was not present in the aqueous suspension with  $\text{TBA}^+/\text{H}^+ \leq 5$ .

On the basis of the above discussion, the osmotic swelling and exfoliation process may be summarized as shown in Figure 12. Layered protonic titanate swells via osmotic hydration when in contact with a large excess of aqueous TBA ions. Intersheet separation increased to  $> 10$  nm when lowering the electrolyte concentration of the suspension. This very high degree of swelling facilitates the exfoliation. A 5-fold excess to an equivalent amount of TBA ions to the exchangeable protons in  $\text{H}_x\text{Ti}_{2-x/4}\square_{x/4}\text{O}_4 \cdot \text{H}_2\text{O}$  is favorable to achieve complete delamination.

The osmotic swelling and exfoliation process were found to be reversible. Ordered swollen crystallites were reconstructed from the exfoliated single sheets by increasing electrolyte content. For example, when an appropriate amount of concentrated TBA hydroxide solution was added to the suspension with

(25) Intersheet separation contracted with time owing to evaporation of water from the sample. The dynamic drying process has been described before.<sup>8</sup>

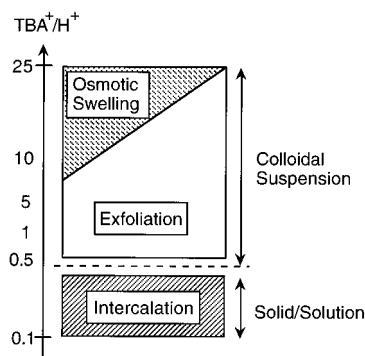


**Figure 12.** Schematic diagram of the osmotic swelling and exfoliation process.

$\text{TBA}^+/\text{H}^+ = 1$  (the completely delaminated sample) to make it 25, the translucent suspension became opalescent. Its X-ray diffraction data was predominantly of an osmotically swollen phase with sharp diffraction lines for a spacing of 4.2 nm, which is equal to that in Figure 2a. This finding implies that swelling and exfoliation are continuous and in equilibrium. It follows that the process involves successive disintegration of the parent crystallites. It deserves mention that the changes in optical absorption features support this progressive cleavage of crystals.

The degradation of exfoliation reaction, seen by the appearance of two crystalline phases for samples with  $\text{TBA}^+/\text{H}^+ \leq 0.3$  (Figures 3 and 4), leads to the conclusion that there is a threshold for delamination. Below this TBA content, no delamination occurred, but the usual intercalation reaction proceeded via solid-to-solution interaction. This is compatible with the changes in UV–visible spectra which suggests a larger particle size for  $\text{TBA}^+/\text{H}^+ \leq 0.3$  (Figure 9).

The threshold at  $\text{TBA}^+/\text{H}^+ = 0.3\text{--}0.5$  approximately coincides with the stoichiometry found for the TBA intercalated titanate of  $(\text{C}_4\text{H}_9)_4\text{N})_{0.3}\text{H}_{0.7}\text{Ti}_{1.825}\text{O}_{1.175}\text{O}_4 \cdot 0.7\text{H}_2\text{O}$  as a freeze-dried product of colloidal suspensions.<sup>14,26</sup> Structural considerations have suggested that TBA ions are closely packed in the gallery.<sup>21</sup> Namely, the threshold corresponds to the steric requirement where the nanosheet surface is effectively covered with TBA ions. Because of the bulky body of TBA ions, only half of the layer charge is neutralized at this composition. Further uptake of TBA ions requires a multilayer arrangement. This situation may trigger a high degree of swelling.

## Conclusion

This study demonstrates that the protonic titanate of  $\text{H}_x\text{Ti}_{2-x/4}\text{O}_4 \cdot \text{H}_2\text{O}$  is a new class of “smectitelike” oxide. High-quality X-ray diffraction data combined with optical absorption properties enabled clarifying how osmotic hydration leads to exfoliation. The electrolyte concentration governed the degree of swelling. The osmotic swollen phase occurred at high electrolyte contents. A decrease in TBA content caused extensive expansion of intersheet separation. The process involved successive cleavage of the layered structure into thinner crystallites and subsequently resulted in exfoliation into single sheets. When the amount of TBA ions was not large enough to cover the surface of the titanate sheet, the system did not become colloidal suspensions but underwent the usual intercalation reaction. These data can shed light on colloid chemistry of platy nanocrystallites as well as the nature of layered materials.

(26) Although suspensions with various TBA concentrations were freeze-dried, the composition of product did not depend on TBA content.

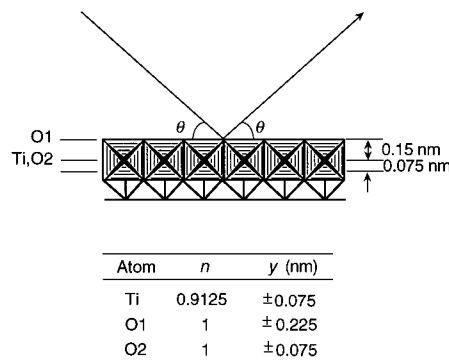


**Figure 13.** Polyhedral representation of the structure for titanate nanosheet. The nanosheet corresponds to the elementary host layer of  $\text{H}_x\text{Ti}_{2-x/4}\text{O}_4 \cdot \text{H}_2\text{O}$ . Positional parameters listed at the bottom are based on the idealized architecture where a  $\text{TiO}_6$  octahedron has a thickness of 0.30 nm.

## Experimental Section

**Synthesis of the Titanate.** A cesium titanate of composition  $\text{Cs}_x\text{Ti}_{2-x/4}\text{O}_4$  ( $x = 0.7$ ) was prepared by firing an intimate mixture of  $\text{Cs}_2\text{CO}_3$  and  $\text{TiO}_2$  (1:5.3 in molar ratio) at 1073 K.<sup>18,27</sup> The chemicals used were of 99.99% purity (Rare Metallic, Co.) and were used without further purification. The calcination of 20 h was repeated twice. The resulting powder (~50 g) was stirred in 2 dm<sup>3</sup> of a hydrochloric acid solution (1 mol dm<sup>-3</sup>) for 24 h. Cs extraction was completed by four cycles of acid exchange. Next, the solid was washed with copious water to remove acid residue. The X-ray diffraction pattern for the air-dried product (Figure 1a) agreed with the data for the protonic oxide of  $\text{H}_x\text{Ti}_{2-x/4}\text{O}_4 \cdot \text{H}_2\text{O}$  reported previously.<sup>18</sup> Observations by scanning electron microscope revealed that the product was of platy microcrystals the dimensions of which were  $\sim 1 \times \sim 1 \times \sim 0.5 \mu\text{m}^3$ .

**Equilibrations.** A weighed amount (0.4 g) of  $\text{H}_x\text{Ti}_{2-x/4}\text{O}_4 \cdot \text{H}_2\text{O}$  was shaken vigorously with an aqueous solution (100 cm<sup>3</sup>) of TBA hydroxide (Wako Jyunkyaku, Co.; Reagent grade),  $(\text{C}_4\text{H}_9)_4\text{NOH}$ , for more than 2 weeks in a thermostated bath regulated at  $298 \pm 0.5$  K. Milli-Q filtered water (Millipore Co.,  $>15 \text{ M}\Omega \text{ cm}^{-1}$ ) was used throughout. The concentration of TBA hydroxide ranged from 0.00165 to 0.412 mol dm<sup>-3</sup>. The amount of TBA hydroxide corresponds to 0.1–25-fold excess to the exchangeable capacity of 4.12 mequiv g<sup>-1</sup> for  $\text{H}_x\text{Ti}_{2-x/4}\text{O}_4 \cdot \text{H}_2\text{O}$  ( $x = 0.7$ ).

**Apparatus.** X-ray diffraction data were collected by a Rigaku Rint-2000S diffractometer with graphite-monochromatized  $\text{Cu K}\alpha$  radiation ( $\lambda = 0.15405$  nm). Measurements were conducted for the colloidal suspensions themselves and also for the colloidal aggregate centrifuged from them at a speed of 15 000 rpm for 30 min. The fluid or colloidal samples were mounted on a horizontal goniometer in a humidity-controllable sample chamber. Relative humidity was kept at 95% to suppress drying of samples, which is necessary to obtain inherent information on colloidal state. Data on colloids were recorded immediately after the centrifugation unless otherwise mentioned.

UV–visible absorption spectra were acquired in a transmission mode using a Hitachi U-4000 spectrophotometer. The original suspensions with a solution-to-solid ratio of 250 cm<sup>3</sup> g<sup>-1</sup> were diluted 333 times to obtain an appropriate range of absorbance.

**Simulations of X-ray Diffraction Profiles.** X-ray diffraction profiles were simulated for the model of *N* titanate sheets in which the intersheet distance of *d* shows Gaussian distribution. Diffraction from this system can be expressed as<sup>28</sup>

(27) (a) Hervieu, M.; Raveau, B. *Rev. Chim. Min.* **1981**, *18*, 642–649. (b) Grey, I. E.; Madsen, I. C.; Watts, J. A.; Bursill, L. A.; Kwiatkowska, J. *J. Solid State Chem.* **1985**, *58*, 350–356. (c) Grey, I. E.; Li, C.; Madsen, I. C.; Watts, J. A. *J. Solid State Chem.* **1987**, *66*, 7–19.

$$I(\theta) = \frac{F^2(\theta)}{N} \left[ N + 2 \sum_{n=1}^{n=N-1} (N-n) \cdot e^{-8\pi^2 n \alpha^2 \sin^2 \theta / \lambda^2} \cdot \cos(4\pi n d \sin \theta / \lambda) \right] \quad (1)$$

where  $\theta$  and  $\lambda$  are the scattering angle and X-ray wavelength, respectively. The parameter,  $\alpha$ , represents a mean-square displacement between neighboring sheets or the standard deviation of Gaussian distribution. The nanosheet structure factor,  $F(\theta)$ , was calculated from

(28) Reynolds, R. C. Jr. *Modern Powder Diffraction*; Bish, D. L., Post, J. E., Eds.; The Mineralogical Society of America: Washington, D.C., 1989; pp 159–163.

the following equation based on the structure shown in Figure 13

$$F(\theta) = 2 \cdot 0.9125 \cdot f_{\text{Ti}} \cdot \cos 2\pi[2 \cdot 0.075 \cdot \sin \theta / \lambda] + 2 \cdot f_{\text{O}} \cdot \cos 2\pi[2 \cdot 0.225 \cdot \sin \theta / \lambda] + 2 \cdot f_{\text{O}} \cdot \cos 2\pi[2 \cdot 0.075 \cdot \sin \theta / \lambda] \quad (2)$$

where  $f_{\text{Ti}}$  and  $f_{\text{O}}$  are the atomic scattering factors for Ti and O atom,<sup>29</sup> respectively. Only cosine parts are considered because the nanosheet is centrosymmetric on projection to the y-axis.

JA974262L

(29) *International Tables for X-ray Crystallography*; The International Union of Crystallography, The Kynoch Press: Birmingham, England, 1968; pp 201–207.